


Logarithmic profiles of velocity in stably stratified atmospheric boundary layers

Yu Cheng ^{*}*Department of Earth and Planetary Sciences, Harvard University, Cambridge, Massachusetts 02138, USA*Andrey Grachev *Boundary Layer Research Team/Atmospheric Dynamics & Analytics Branch,
DEVCOM Army Research Laboratory, WSMR, New Mexico 88002, USA*

Chiel van Heerwaarden

Meteorology and Air Quality Group, Wageningen University, Wageningen 6700 AA, The Netherlands

(Received 1 August 2023; accepted 20 October 2023; published 16 November 2023)

The universal velocity log law proposed by von Kármán in wall-bounded turbulent flows is one of the cornerstones of turbulence theory. When buoyancy effects are important, the universal velocity log law is typically believed to break down according to Monin-Obukhov similarity theory (MOST), which has been used in almost all global weather and climate models to describe the dependence of the mean velocity profiles on buoyancy near the earth's surface and to characterize the surface-atmosphere exchange of momentum, heat, water vapor, and carbon dioxide. In contrast to MOST, we propose logarithmic profiles of near-wall mean velocity in the stably stratified atmospheric boundary layers based on direct numerical simulations and field observations across a wide range of buoyancy effects. We find that buoyancy does not seem to change the logarithmic nature of velocity profiles but instead modifies the slope of the log law in stably stratified conditions. This paper provides a perspective on wall turbulence and can be applied to numerical simulations of turbulence, weather, and climate.

DOI: [10.1103/PhysRevFluids.8.114602](https://doi.org/10.1103/PhysRevFluids.8.114602)

I. INTRODUCTION

Wall-bounded turbulent flows are commonly observed, for example, as flow through pipes and ducts, flow near the earth's surface or around a vehicle, and water flow in rivers. The understanding of wall-bounded turbulence may thus contribute to engineering designs and geophysical predictions. In wall-bounded turbulent flows, there exists a universal logarithmic velocity profile [1,2] near the wall, characterized by a linear relation between mean velocity and the logarithm of the distance to the wall. We note that a power law might also potentially capture the velocity distribution near the wall [3,4], but here we focus on the response of the log law to buoyancy effects. The universal velocity log law has been supported by laboratory measurements of pipe flow [5] and boundary layer [6], atmospheric observations [7], and direct numerical simulations (DNSs) [8,9] of turbulent shear flows. When wall-bounded turbulence is influenced by buoyancy, the mean velocity may not be adequately described by the universal log law. To address the buoyancy effects, Monin-Obukhov similarity theory (MOST) was proposed to revise the universal velocity log law

*yc2965@columbia.edu

using stability correction functions of the distance to the wall z and the Obukhov length [10] L based on dimensional analysis [11]. MOST has been used to describe buoyancy corrections of the mean velocity profile and to provide velocity and momentum flux in the atmospheric surface layer, roughly the lowest 10% of the atmospheric boundary layer (ABL), roughly the lowest 1 km of the atmosphere [12], in almost all numerical weather prediction and climate models [13–16].

Stably stratified conditions are frequently observed over land at night [17] and in polar regions of the earth [18] when the air is cooled by the land surface. Stably stratified turbulence in the ABL is very difficult to be represented [19–23] in numerical weather prediction and climate models [24–26]. The turbulence representation in the ABL is especially important for the Arctic as climate change is amplified there [27]. The difficulty of representing stably stratified turbulence [24–26] is partly due to the widely known failure of MOST in the atmospheric surface layer in very stable conditions [17,28]. In particular, MOST does not capture the mean velocity profile when buoyancy-driven stratification is significant as shown in field observations of the strongly stratified ABL [29–34].

Based on a reformulation of MOST, Grachev *et al.* [18] proposed a similarity theory using the Dougherty-Ozmidov length scale L_O [35,36], which is typically regarded as the outer scale of isotropic turbulence in stably stratified conditions [37–40]. It is thus possible that some important length scales might be missing in the dimensional analysis of MOST when stably stratified turbulence is considered, as shown in convective conditions [41,42]. The strength of stratification is typically described by the stability parameter z/L according to MOST, where $L = \frac{u_*^3}{\frac{\kappa g}{\Theta_r} u_* \theta_*}$, u_* is the friction velocity, κ is the von Kármán constant ($\kappa = 0.4$ in this paper), g is the gravitational acceleration, Θ_r is a reference potential temperature, $\theta_* \equiv \frac{\nu_\theta}{u_*} \frac{\partial \Theta}{\partial z} |_{z=0}$ is a scaling temperature, and ν_θ is the thermal diffusivity. When buoyant stratification increases, z/L increases. In addition, Grachev *et al.* [18] showed that z/L_O may also characterize buoyancy effects, where L_O is the Dougherty-Ozmidov length scale [35,36].

It is worth noting that the collapse of turbulence in stably stratified conditions can be indicated by the parameter $\frac{L}{\delta_v} = \frac{L u_*}{\nu}$ [43], where δ_v is the viscous length scale and ν is the kinematic viscosity. L/δ_v can characterize both buoyancy effects (i.e., the inverse of gradient Richardson number) [44] and Reynolds number effects (i.e., the scale separation between L and δ_v) [43]. We can write $\frac{L}{\delta_v} = \frac{z_i/\delta_v}{z_i/L}$, where z_i is the boundary layer height. $\frac{z_i}{\delta_v} = \frac{u_* z_i}{\nu}$ can represent Reynolds number effects, and $\frac{z_i}{L}$ can represent buoyancy effects (e.g., in the convective boundary layer [42]). We will show that $\frac{z_i}{\delta_v}$ and $\frac{z_i}{L}$ can be used to constrain the slope of our proposed velocity log law.

Recently, logarithmic temperature profiles have been reported in the near-wall regions of turbulent Rayleigh-Bénard convection [45], vertical natural convection [46], and convective ABL [42], which is in contrast with the breakdown of a log law according to MOST. Thus, the logarithmic nature does not necessarily break down under the influence of buoyancy, which was a hypothesis made by Budyko, although no numerical or experiment support was presented. In particular, Budyko [47] assumed that the logarithmic boundary layer may still exist under stratification effects if the von Kármán universal constant is replaced by a function of stratification. In this paper, we aim to investigate the existence of logarithmic velocity profiles in the stably stratified ABL and the possible dependence of velocity profiles on other stability parameters (or length scales) using high-resolution DNS experiments and field observations.

II. METHODS

A. Direct numerical simulations

Large eddy simulations (LESs) [48] have been widely used to study the ABL. However, subgrid-scale turbulence models [49] may lead to uncertainties near the wall and LESs might have difficulties in simulating strongly stratified turbulence [43]. In addition, wall-modeled LESs for the ABL usually invokes MOST [50]. Moreover, turbulence spectra are often not well resolved [40] since the Dougherty-Ozmidov scale is typically not resolved in LESs [38] except possibly in a few studies [51]. Recently, DNS has been used to study the stably stratified ABL [40,43,44,52,53],

although the Reynolds number is not as high as that in the real ABL. To obtain high-resolution velocity profiles in the near-wall region, DNSs of the stably stratified Ekman layers are conducted in this study.

The incompressible Navier-Stokes equations with Boussinesq approximation are solved [54]. Periodic boundary conditions are employed in the horizontal (x and y) directions. First, we simulate a turbulent Ekman layer flow [55] over a smooth surface in the absence of buoyancy as in previous studies [52,53]. The three simulations of neutral Ekman layer flow named ReD900, ReD1800, and ReD2700 are forced with varying mean geostrophic wind. The grid points are $320 \times 320 \times 1664$ for data set ReD900, $640 \times 640 \times 3328$ for data set ReD1800, $960 \times 960 \times 4992$ for dataset ReD2700 in streamwise (x), spanwise (y), and vertical directions (z), respectively. The Reynolds number is $Re_D = \frac{U_g D}{\nu}$, where U_g is the geostrophic wind speed, $D = (2\nu/f)^{1/2}$ is the laminar Ekman layer depth, ν is the kinematic viscosity, and f is the Coriolis parameter ($f = 10^{-4}$ rad s $^{-1}$ in this paper). Similarly to previous experiments [52,53], a neutral velocity log law of the Ekman layer is obtained after $ft = 5.9, 6.0$ and 13.6 for ReD900, ReD1800, and ReD2700, respectively. Then we add a cooling surface buoyancy flux B_0 to generate various stably stratified conditions. The boundary conditions for the temperature field are zero heat flux at the top of the computational domain. At the top 25% of the computation domain, a sponge layer is added to prevent reflection of gravity waves by adding a relaxation term that damps fluctuations at a prescribed relaxation timescale to the equations of motion [56]. The near-surface stability is measured by normalized Obukhov length $L^+ = \frac{L}{\delta_v} = \frac{u_\tau^3}{\frac{\kappa g}{\Theta_r} u_\tau \theta_*} \frac{u_\tau}{\nu}$. The initial $L^+(t = 0)$ is used to measure the strength of imposed stratification, which is computed from u_τ in the neutral Ekman layer before the cooling surface buoyancy flux B_0 is applied. Details of the DNS setup can be found in Cheng *et al.* [40] and the open-source code (named MicroHH) is described in Heerwaarden *et al.* [54].

We note that turbulence decays fast in the stably stratified Ekman layer [53], thus we only analyze the periods when $\frac{L_0}{\eta} > 1$ for the possible existence of Kolmogorov's energy cascade [40], where $L_0 = 2\pi(\epsilon/N^3)^{1/2}$ is the Dougherty-Ozmidov scale [35,36,38,40], $\eta = (\nu^3/\epsilon)^{1/4}$ is the Kolmogorov scale [57], and ϵ is the turbulent kinetic energy dissipation rate. Kolmogorov's energy cascade characterizes an equilibrium state of turbulent flows at sufficiently high Reynolds numbers, where statistics of turbulence can be universally described by a few physical variables. When Kolmogorov's energy cascade is absent, the equilibrium state breaks down and turbulence statistics might not be simply described by a few parameters in a universal way. Therefore, we focus on the condition when there still exists an equilibrium state. It is worth noting that $\frac{L_0}{\eta} > 1$ is still a rough proxy for an equilibrium state of turbulent flows. The velocity profiles might not be simply described by a few parameters when there is no Kolmogorov's energy cascade in stably stratified conditions and will be investigated in a future study. The nondimensional averaging time $t_a = ft$ for our velocity profiles is on the order of 0.02, which is much smaller than the averaging period ($ft = \pi$) in Shah and Bou-Zeid [52]. The friction Reynolds number $Re_\tau = u_\tau \delta_t / \nu$ at the selected time step of the DNS experiments ReD900 ($L^+ = 160$), ReD1800 ($L^+ = 800$), ReD1800 ($L^+ = 3200$), and ReD2700 ($L^+ = 160$) are 861, 1208, 1026, and 3122, respectively, where $\delta_t = u_\tau / f$ is the turbulent Ekman layer length scale. Following the suggestion of Shah and Bou-Zeid [52], we compute the boundary layer height z_i in DNS experiments as the height where maximum of velocity occurs. We note that other definitions of stable boundary layer (SBL) height has been proposed as there might not be a strong demarcation at the top of SBL [12]. The defined SBL height in our study captures the fact that flow speed in the boundary layer can be higher than the geostrophic value far from the wall [12] and is an example of SBL height defined in Stull [12]. The eight stably stratified DNS experiments are described in Table I.

B. Field observations

A tower of 213 m has been installed in the Cabauw Experimental Site for Atmospheric Research (CESAR) [58] (4.926° E, 51.97° N) in The Netherlands, where multilevel turbulence observations

TABLE I. Key parameters of simulated stably stratified ABLs. $\text{Re}_\tau = \frac{u_\tau \delta_i}{\nu}$ is the friction Reynolds number, u_τ is the friction velocity, δ_i is the turbulent Ekman layer length scale, ν is the kinematic viscosity, z_i is the boundary layer height determined from the height where maximum of velocity occurs, L is the Obukhov length, and L_x , L_y , and L_z are the domain sizes in the x , y , and z directions, respectively. Δ_x^+ (Δ_y^+) and Δ_z^+ are the spatial grid resolutions denoted by inner units in the x , y , and z directions, respectively. κ_u is the inverse of the velocity log law slope. The range of velocity log law is also indicated using z^+ and $\frac{z}{L}$.

Re_D	$\text{Re}_\tau = \frac{u_\tau \delta_i}{\nu}$	$\frac{z_i}{L}$	Δ_x^+ (Δ_y^+)	Δ_z^+	L^+	κ_u	Log-law range in z^+	Log-law range in $\frac{z}{L}$
900	861	5.4	6.5	0.82	160	0.33	81 ~ 100	1.01 ~ 1.25
900	806	2.2	6.3	0.80	480	0.28	59 ~ 70	0.30 ~ 0.35
900	548	0.9	5.2	0.66	1600	0.28	83 ~ 94	0.26 ~ 0.30
1800	1208	6.6	3.8	0.49	800	0.20	81 ~ 97	0.84 ~ 1.01
1800	1088	2.0	3.6	0.46	1600	0.17	86 ~ 103	0.55 ~ 0.66
1800	1026	3.7	3.5	0.45	3200	0.16	112 ~ 131	0.40 ~ 0.47
2700	3122	42.0	4.1	0.52	160	0.24	100 ~ 121	3.04 ~ 3.67
2700	1624	11.2	3.0	0.38	1600	0.15	102 ~ 122	1.16 ~ 1.38

at 10 m, 20 m, 40 m, 80 m, 140 m, and 200 m above a grass field are available in the ABL. We downloaded a number of 30-minute data segments between 1:00 and 5:00 UTC in July, 2019, from the CESAR data archive as the raw data, which has been quality controlled [58]. These include velocity measurements from cup-anemometers at multiple levels and surface flux measurements from sonic anemometers at 3 m. Wind profilers were not routinely available at the Cabauw site. Lidars (including ceilometers) and wind profilers were shown to obtain similar boundary layer heights [59], although lidar backscatter is proportional to aerosol content and wind profiler backscatter depends on the refractive index structure. Through detecting the top of an elevated aerosol layer, the boundary layer height z_i is measured by the Lufft CHM 15 k ceilometer [60]. We calculate the average ABL height over each 30-minute segment as the raw data.

The raw data satisfying the following two conditions are further used to characterize the velocity profile: (1) the mean surface heat flux in the 30-minute sampling period has to be negative (i.e., heat transferred from air to ground) and (2) the boundary layer height z_i is larger than 800 m. The first condition is used to select stably stratified ABL. The second condition is used to ensure that we include as many measurements as possible (especially those at 200 m) within the atmospheric surface layer through prescribing large boundary layer height z_i . These two conditions lead to 40 different stably stratified 30-minute periods. Although extremely stratified conditions are eliminated by the z_i requirement, there are still a few observations of the strongly stratified ABL, as shown in Fig. 3.

III. RESULTS

A. Existence of a velocity log law

The normalized mean velocity $\frac{U}{u_\tau}$ seems to fit a log law with $z^+ \equiv \frac{z}{\delta_v}$ in the DNS data sets (Fig. 1). The coefficient of determination R^2 for $\frac{U}{u_\tau}$ and $\ln(z^+)$ is 1.00 for the selected vertical layer (according to Fig. 2) near the wall across the DNS data sets. Following Lee and Moser [8], we use a plateau of $\frac{z}{u_\tau} \frac{\partial U}{\partial z}$ to more clearly indicate the existence of a velocity log law (Fig. 2). The black dashed line (plateau) in Fig. 2 is used to characterize the vertical layer where the velocity log law is identified (as detailed in Table I).

In the identified log law layer, the variations of turbulent momentum flux $\overline{w'u'}$ defined as $\frac{\max(\overline{w'u'}) - \min(\overline{w'u'})}{\max(\overline{w'u'})}$ are 4.7% (ReD900, $L^+ = 160$), 10.6% (ReD1800, $L^+ = 800$), 5.3% (ReD1800, $L^+ = 3200$), and 4.3% (ReD2700, $L^+ = 160$), respectively. This is consistent with the definition of

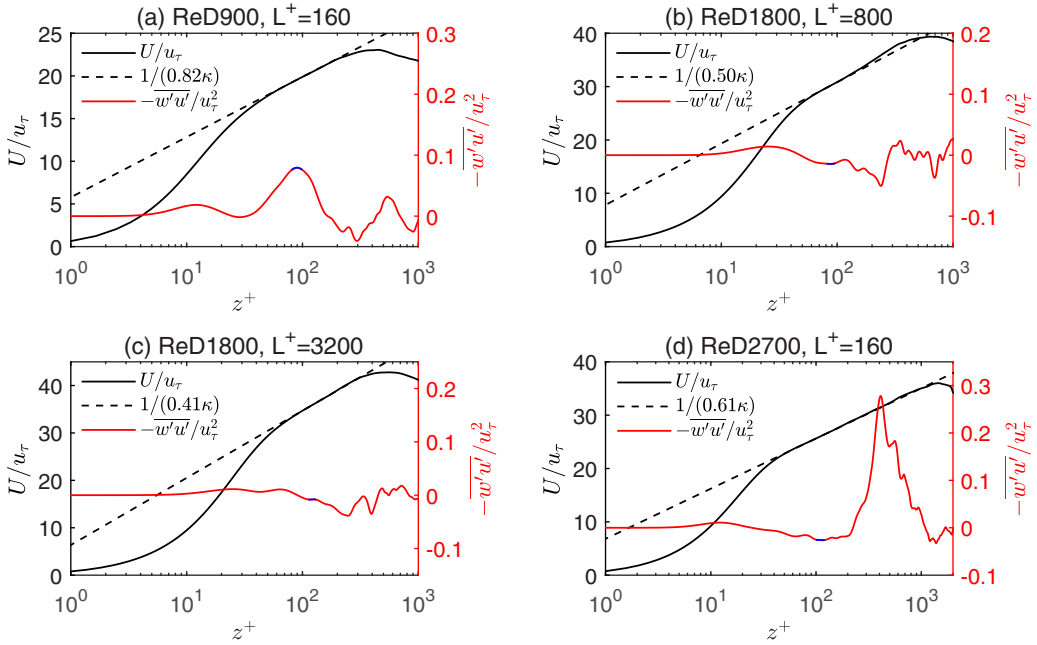


FIG. 1. Normalized velocity U/u_τ and momentum flux $-\overline{w'u'}/u_\tau^2$ in the vertical direction of the DNS experiments. The blue line denotes the normalized momentum flux $-\overline{w'u'}/u_\tau^2$ in the velocity log law region.

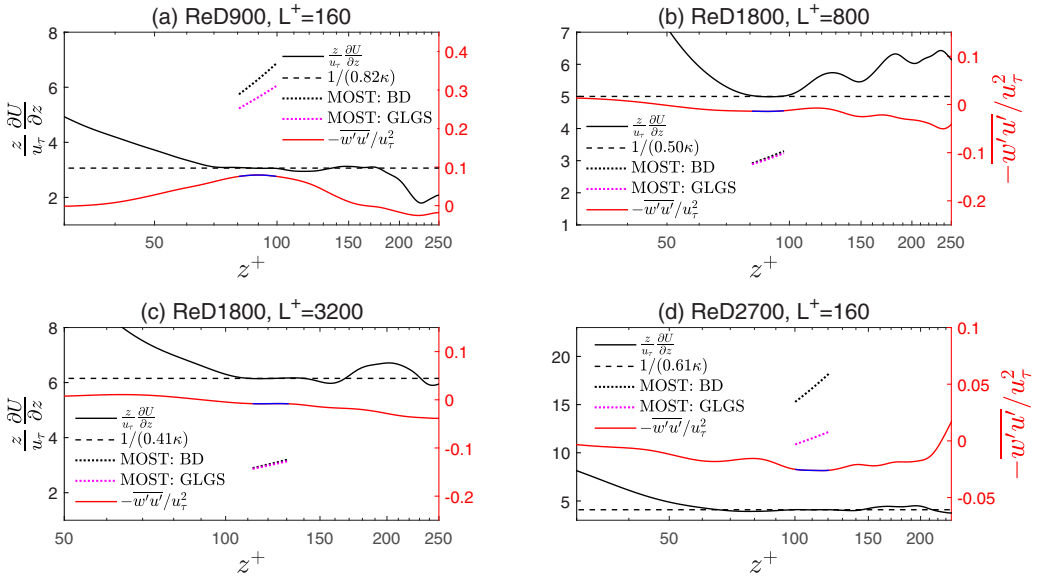


FIG. 2. Vertical profiles of normalized velocity gradient ($z/u_\tau \partial U / \partial z$) (equal to $1/\kappa_u$) in DNS data sets. The Monin-Obukhov similarity functions of Businger *et al.* [68] denoted by MOST: BD and Gryanik *et al.* [70] denoted by MOST: GLGS are also shown. The Businger *et al.* [68] formula: $\frac{z}{u_\tau} \frac{\partial U}{\partial z} = \frac{1}{\kappa} (1 + 4.7 \frac{z}{L})$. The Gryanik *et al.* [70] formula: $\frac{z}{u_\tau} \frac{\partial U}{\partial z} = \frac{1}{\kappa} (1 + \frac{5.0z/L}{(1+0.3z/L)^{2/3}})$.

constant-flux layer [12], where flux variations are on the order of 10%. This constant momentum flux zone is similar to the atmospheric surface layer, where the variation of turbulent fluxes should scale with the ratio of the atmospheric surface layer height to the ABL height [61], roughly 10%. The coexistence of a velocity log law and constant momentum flux in the DNS data sets (Fig. 1) resembles that in turbulent shear flows [62]. It is worth noting that countergradient momentum flux is found in Fig. 1, which is not surprising given the relatively short analyzed period (as turbulence decays fast in DNS experiments). Countergradient turbulent fluxes have been observed in stably stratified boundary layers in previous studies [63–66].

As shown in Table 1, the range of Reynolds number of the DNS experiments is $548 \leq \text{Re}_\tau \leq 3122$ or, equivalently, $276 \leq z_i/\delta_v \leq 1345$. The vertical layers of velocity log law vary in different DNS experiments but all fall in the range $59 \leq z^+ \leq 122$. According to Marusic *et al.* [67], the universal velocity log law of turbulent shear flows in the absence of buoyancy effects is found in the range $3(z_i/\delta_v)^{1/2} < z^+ < 0.15z_i/\delta_v$, which corresponds to $50 \leq z^+ \leq 202$ in our DNS experiments. Thus, the range of the stably stratified velocity log law roughly falls within that of neutral velocity log law, although the influence of buoyancy effects cannot be neglected in our DNS experiments. In addition, the stably stratified velocity log law is found when $\frac{z}{L} > 3$ (in ReD2700, $L^+ = 160$) using the MOST stability parameter. However, the MOST stability correction functions proposed by both Businger *et al.* [68] and Gryanik *et al.* [70] suggest that velocity profiles will significantly deviate from a log law in such stably stratified conditions [Fig. 2(d)]. In fact, the stability correction functions of MOST proposed by Businger *et al.* [68] are only defined in the range $0 < \frac{z}{L} < 1$ in stably stratified conditions due to its poor behavior in more stratified conditions [71]. Therefore, the proposed velocity log law is fundamentally different from MOST and might be applied to a wider range of buoyant conditions.

The slopes of the proposed velocity log law are $\frac{1}{0.82\kappa}$ (ReD900, $L^+ = 160$), $\frac{1}{0.50\kappa}$ (ReD1800, $L^+ = 800$), $\frac{1}{0.41\kappa}$ (ReD1800, $L^+ = 3200$), and $\frac{1}{0.61\kappa}$ (ReD2700, $L^+ = 160$), respectively (Fig. 1). In comparison, the slope of the universal log law for mean velocity in turbulent shear flows is constant [67], i.e., $\frac{1}{\kappa}$. The variations of the slope of the proposed velocity log law is due to buoyancy effects as well as Reynolds number effects. Similar dependence of the slope on buoyancy has been found in temperature log laws in the convective boundary layers [42] and Rayleigh-Bénard convection [45]. The slope of the proposed velocity log law will be revisited later.

In addition to the DNS experiments, we analyze field observations of the stably stratified ABL in the Cabauw experiment, which are at higher Reynolds number ($1.4 \times 10^6 \leq \frac{z_i}{\delta_v} \leq 2.1 \times 10^7$). A linear relation is fitted between the normalized velocity $\frac{U-U_{h1}}{u_\tau}$ and $\ln(z^+)$ in the four sampled periods (Fig. 3), where U is the temporally averaged wind speed at heights of 20 m, 40 m, 80 m, 140 m, and 200 m in a 30-minute period, and U_{h1} is the averaged wind speed at 10 m. The coefficient of determination for $\frac{U-U_{h1}}{u_\tau}$ and $\ln(z^+)$ falls in the range $R^2 > 0.88$ in all 40 selected periods (see Supplemental Material [69] for more atmospheric observations), indicating the linear relation between $\frac{U-U_{h1}}{u_\tau}$ and $\ln(z^+)$ and thus the presence of a velocity log law. We also compare the velocity profile based on MOST [68,70,72,73] with field observations. There are substantial deviations in the MOST function proposed by Businger *et al.* [68] across stably stratified conditions in the range $0.22 \leq z/L \leq 15.68$ (Fig. 3), where $z = 10$ m (at one vertical level of tower observations). The MOST function proposed by Gryanik *et al.* [70] decreased the errors in the velocity prediction from Businger *et al.* [68], especially in more stably stratified conditions. However, Gryanik *et al.* [70] still misses the plateau of $\frac{z}{u_\tau} \frac{\partial U}{\partial z}$ in DNS experiments (Fig. 2), which is a more stringent test of the log law. The field observations in the real ABL also seem to imply the possible existence of the velocity log law observed in our DNS experiments.

It is worth noting that few studies have investigated the logarithmic nature of the mean velocity profile in the stably stratified ABL. This is partly due to the sparse measurements in the vertical direction and lack of ABL height measurements [33,74]. In addition, large uncertainties remain in the observations of the stable ABL since instruments often operate near their threshold levels due to small turbulence intensities [75,76]. Unlike DNS experiments, a plateau of $\frac{z}{u_\tau} \frac{\partial U}{\partial z}$ can hardly be

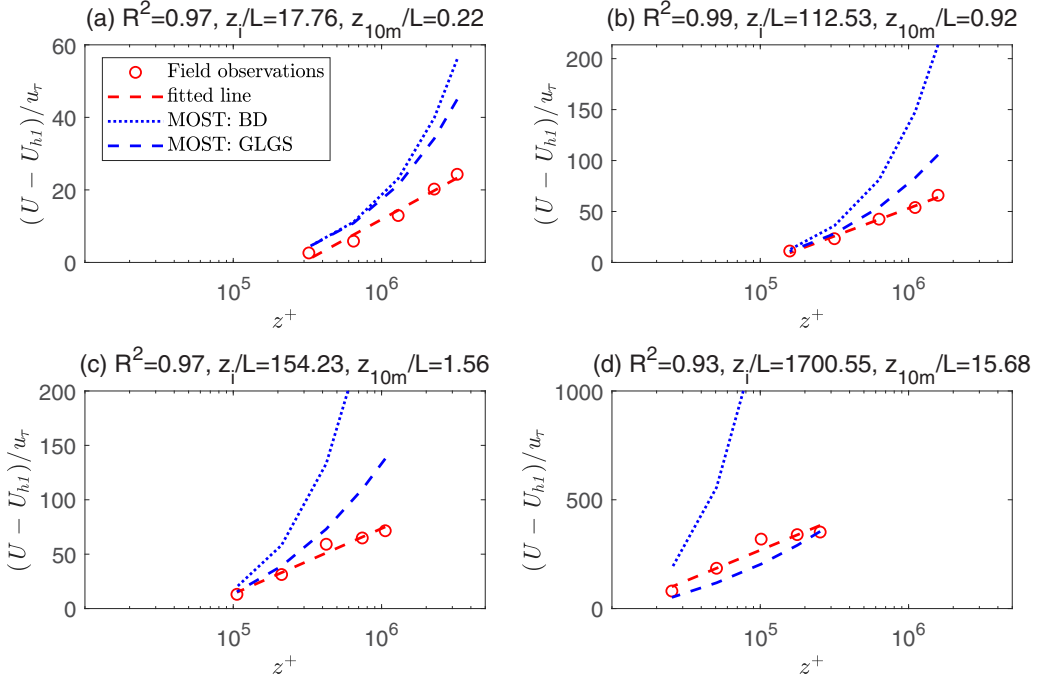


FIG. 3. Normalized velocity $\frac{U - U_{hl}}{u_{\tau}}$ in the vertical direction of Cabauw observations. R^2 denotes the coefficient of determination for $\frac{U - U_{hl}}{u_{\tau}}$ and $\ln(z^+)$, and z_{10m}/L denotes the stability parameter z/L at the height 10 m. MOST: BD and MOST: GLGS denote the computed velocity profiles based on Businger *et al.* [68] and Gryanik *et al.* [70], respectively.

identified in field observations to support a velocity log law. Moreover, field observations are often analyzed within the framework of MOST since MOST is still regarded as the foundation of ABL turbulence theory [71].

B. Slope of the velocity log law

1. Dimensional analysis

The fully developed stably stratified boundary layer flow can be described by v , u_{τ} , z , θ_* , and the boundary layer height z_i . To compute the mean velocity U , we need to write $f(U, v, u_{\tau}, z, \theta_*, z_i) = 0$, where f is a function to be determined. These six variables can form three independent physical dimensions: velocity, length, and temperature. According to the Buckingham Pi theorem, the above equation can be written as $6 - 3 = 3$ dimensionless parameters. These variables can form three nondimensional groups:

$$\frac{z}{L} = \frac{\kappa g \theta_*}{\Theta_r} \frac{z}{u_{\tau}^2}, \quad (1)$$

$$\frac{z_i}{L} = \frac{\kappa g \theta_*}{\Theta_r} \frac{z_i}{u_{\tau}^2}, \quad (2)$$

and

$$\frac{z_i}{\delta_v} = \frac{u_{\tau} z_i}{v}. \quad (3)$$

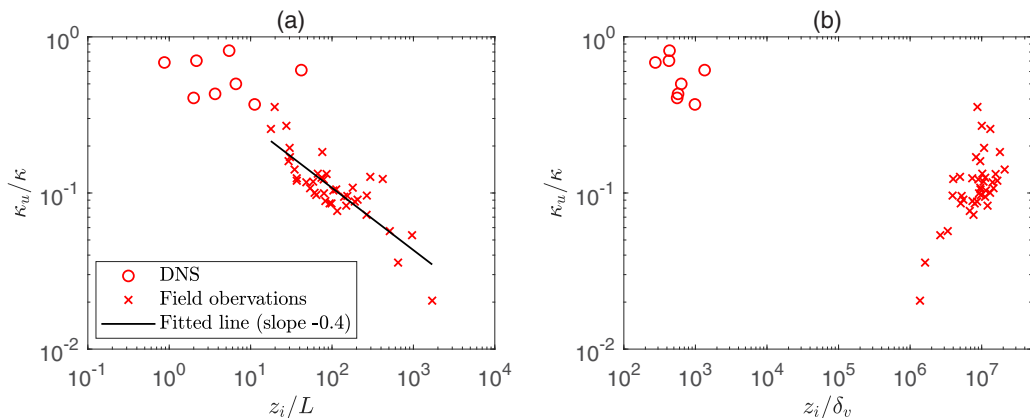


FIG. 4. The ratio $\frac{\kappa_u}{\kappa}$ plotted against (a) $\frac{z_i}{L}$, and (b) $\frac{z_i}{\delta_v}$ under various stably stratified conditions in DNS experiments and Cabauw observations. The linear fit (with a coefficient of determination $R^2 = 0.7$) for the field observations is also shown in (a).

The mean velocity profile can be written as

$$U = u_\tau F_0\left(\frac{z}{L}, \frac{z_i}{L}, \frac{z_i}{\delta_v}\right), \quad (4)$$

where F_0 is a function of $\frac{z}{L}$, $\frac{z_i}{L}$, and $\frac{z_i}{\delta_v}$. Following the argument for velocity gradient in Pope (2000) [77], $\frac{\partial U}{\partial z}$ can be written as

$$\frac{\partial U}{\partial z} = \frac{u_\tau}{z} \Phi\left(\frac{z}{L}, \frac{z_i}{L}, \frac{z_i}{\delta_v}\right). \quad (5)$$

According to the DNS data sets, $\frac{z}{u_\tau} \frac{\partial U}{\partial z}$ is independent of z in the log law region. For the existence of a velocity log law, Φ has to be independent of $\frac{z}{L}$, leading to

$$\frac{\partial U}{\partial z} = \frac{u_\tau}{z} \Phi\left(\frac{z_i}{L}, \frac{z_i}{\delta_v}\right). \quad (6)$$

We denote $\frac{1}{\kappa_u} \equiv \Phi\left(\frac{z_i}{L}, \frac{z_i}{\delta_v}\right)$ and obtain

$$\frac{\partial U}{\partial z} = \frac{u_\tau}{z} \frac{1}{\kappa_u}. \quad (7)$$

After integration from a reference height z_r to z , we have

$$\frac{U - U_{z_r}}{u_\tau} = \frac{1}{\kappa_u} \ln\left(\frac{z}{z_r}\right). \quad (8)$$

Equation (8) is just the velocity log law since κ_u is independent of z and is a function of $\frac{z_i}{L}$ and $\frac{z_i}{\delta_v}$. This dimensional analysis points out the relevant parameters that determine the slope of the proposed velocity log law, which should be calibrated from numerical experiments or field observations.

2. DNS and field observations

The DNS and Cabauw data sets suggest that κ_u/κ decreases nonlinearly with increasing z_i/L [Fig. 4(a)]. That is, as buoyancy effects increase (i.e., z_i/L increases), the slope of the stably stratified velocity log law deviates more from that of the neutral channel flow.

When z_i/δ_v increases from $\sim 10^3$ (DNS data sets) to $\sim 10^7$ (field observations), κ_u/κ does not seem to show a monotonic trend [Fig. 4(b)]. At high Reynolds number ($1.4 \times 10^6 \leq z_i/\delta_v \leq 2.1 \times 10^7$), κ_u/κ in Cabauw observations can be assumed to be independent of Reynolds number; thus buoyancy effects dominates. In comparison, the Reynolds number is $276 \leq z_i/\delta_v \leq 1345$ for the DNS data sets, thus there is a wide separation of Reynolds number between field observations and DNS experiments. The range of MOST stability parameters in the identified log law range are $0.22 < z/L < 313.70$ and $0.26 < z/L < 3.67$ for the Cabauw and DNS data sets, respectively. Therefore, both larger Reynolds number and stronger buoyancy effects can be found in Cabauw observations. More accurate measurements of turbulent fluxes and denser measurements of velocity in the vertical direction over a wider range of Reynolds numbers and stably stratified conditions as well as laboratory experiments (e.g., Williams *et al.* [78]) will better constrain κ_u in the ABL. For example, a plateau of $\frac{z}{u_\tau} \frac{\partial U}{\partial z}$ seemed to be observed in the laboratory experiments of stably stratified turbulent boundary layers in Williams *et al.* [78], although the existence of a log law was not stated explicitly.

3. Asymptotic analysis

At sufficiently high Reynolds numbers like the field observations, we conduct asymptotic analysis for the slope κ_u in the neutral limit and strongly stratified limit by neglecting the Reynolds number effects.

In the neutral limit (where there is no buoyancy) at sufficiently high Reynolds numbers, $z_i/L \rightarrow 0$, we expect that $\kappa_u/\kappa \rightarrow 1$ since von Kármán's universal log law is recovered.

In the strongly stratified limit at sufficiently high Reynolds numbers, $z_i/L \rightarrow \infty$ and $u_\tau \rightarrow 0$. Here z_i refers to the lowest height where wind speed is maximum, which is one of the definitions of SBL height in Stull [12]. Thus, z_i is different from the neutral Ekman layer height, which is typically proportional to u_τ/f [79,80]. The following asymptotic relation is required to cancel out u_τ to ensure nonzero $\frac{\partial U}{\partial z}$:

$$\Phi\left(\frac{z_i}{\delta_v}, \frac{z_i}{L}\right) = \Phi\left(\frac{z_i}{L}\right) = c_1 \left(\frac{\kappa g z_i \theta_*}{\Theta_r u_\tau^2}\right)^{1/2} \quad \text{for } \frac{z_i}{L} \rightarrow \infty, \quad (9)$$

where c_1 is a constant. Then the velocity gradient $\partial U/\partial z$ can then be rewritten as

$$\frac{\partial U}{\partial z} = c_1 \left(\frac{\kappa g z_i}{\Theta_r}\right)^{1/2} \frac{\theta_*^{1/2}}{z} \quad \text{for } \frac{z_i}{L} \rightarrow \infty. \quad (10)$$

The above equation suggests that $\partial U/\partial z \rightarrow \infty$ as $z_i/L \rightarrow \infty$ and $\theta_* \rightarrow \infty$, corresponding to extreme stratified conditions. As $\kappa_u = 1/\Phi$, we can obtain

$$\kappa_u = \frac{1}{c_1} \left(\frac{z_i}{L}\right)^{-1/2} \quad \text{for } \frac{z_i}{L} \rightarrow \infty. \quad (11)$$

The slope between κ_u and z_i/L obtained from Cabauw observations in the log-log plot is around -0.4 [Fig. 4(a)], which is not exactly the same as $-1/2$ based on the above equation. However, the asymptotic analysis still qualitatively captures the relation between κ_u and z_i/L in extreme stratified conditions at sufficiently high Reynolds number. It is worth noting that the extreme condition $z_i/L \rightarrow \infty$ is not observed in the Cabauw experiments, which might also be influenced by measurement uncertainties, thus leading to the difference between the observations and asymptotic analysis.

C. Discussion

The proposed velocity log law in the stably stratified boundary layers can be written as $\frac{\kappa_u z}{u_\tau} \frac{\partial U}{\partial z} = 1$ or, equivalently,

$$\frac{\kappa z}{u_\tau} \frac{\partial U}{\partial z} = \kappa \Phi\left(\frac{z_i}{L}, \frac{z_i}{\delta_v}\right) = \frac{\kappa}{\kappa_u}, \quad (12)$$

where $\Phi\left(\frac{z_i}{L}, \frac{z_i}{\delta_v}\right)$ is independent of z and needs to be determined by numerical experiments or observations. According to MOST, the normalized velocity gradient was instead assumed to depend on z/L [11],

$$\frac{\kappa z}{u_\tau} \frac{\partial U}{\partial z} = \phi_m\left(\frac{z}{L}\right), \quad (13)$$

where ϕ_m is a stability correction function dependent on the distance to the wall z , thus leading to a nonlogarithmic profile. The widely used Businger profile [68] and GLGS profile [70] for MOST are shown in Fig. 2, which are both characterized by a slope rather than the observed plateau for $\frac{\kappa z}{u_\tau} \frac{\partial U}{\partial z}$. In numerical experiments, the function $\Phi\left(\frac{z_i}{L}, \frac{z_i}{\delta_v}\right)$ does not depend on z , thus leading to a log law. In our various stably stratified DNS datasets, $\frac{\kappa z}{u_\tau} \frac{\partial U}{\partial z}$ approaches a constant that is equal to $\frac{\kappa}{\kappa_u}$ (Fig. 2), thus supporting the possible existence of a log law rather than MOST. In addition, the slope of the proposed velocity log law depends on $\frac{z_i}{L}$ (buoyancy effects) and $\frac{z_i}{\delta_v}$ (Reynolds number effects). Such dependence of the slope on $\frac{z_i}{L}$ and $\frac{z_i}{\delta_v}$ has also been reported in temperature profiles in the convective boundary layers [42].

IV. CONCLUSION

We report logarithmic velocity profiles in wall-bounded turbulence influenced by buoyancy effects, through dimensional analysis, DNS experiments, and field observations of the stably stratified boundary layers. This velocity log law can be described by $\frac{\kappa_u z}{u_\tau} \frac{\partial U}{\partial z} = 1$, where κ_u is a function of $\frac{z_i}{L}$ (buoyancy effects) and $\frac{z_i}{\delta_v}$ (Reynolds number effects), as suggested by both DNS experiments and field observations. Therefore, the logarithmic nature of velocity profiles seems to remain valid when stably stratified buoyancy effects are important in wall-bounded turbulence. Asymptotic analysis for the slope κ_u has been conducted in the neutral limit and strongly stratified limit at sufficiently high Reynolds numbers. More accurate observations over a wider range of Reynolds numbers and stably stratified conditions may better constrain κ_u in the atmosphere. The proposed velocity log profile may serve as an alternative to Monin-Obukhov similarity function for velocity in global climate models and wall models for LESs, possibly leading to more realistic predictions of weather, climate, and hydrology, especially in polar regions.

ACKNOWLEDGMENTS

We thank Dr. K. McColl for helpful discussions. The computations in this paper were run on the FASRC Cannon cluster supported by the FAS Division of Science Research Computing Group at Harvard University. We would like to thank Dr. F. C. Bosveld and H. Klein Baltink for help in obtaining the field data at the Cabauw Experimental Site for Atmospheric Research [81].

-
- [1] T. von Kármán, Mechanische Ähnlichkeit und turbulenz, *Nachr. Ges. Wiss. Goettingen, Math.-Phys. Kl.* 58 (1930); Mechanical similarity and turbulence, *Proc. 3. Int. Cong. Appl. Mech* 322 (1930), pp. 58–76.
 - [2] C. B. Millikan, A critical discussion of turbulent flow in channels and circular tubes, in *Proceedings of the Fifth International Congress for Applied Mechanics* (Wiley, Cambridge, MA, 1938), pp. 386–392.

- [3] G. Barenblatt, Scaling laws for fully developed turbulent shear flows. Part 1. Basic hypotheses and analysis, *J. Fluid Mech.* **248**, 513 (1993).
- [4] A. J. Smits, Batchelor prize lecture: Measurements in wall-bounded turbulence, *J. Fluid Mech.* **940**, A1 (2022).
- [5] B. J. McKeon, J.-D. Li, W. Jiang, J. F. Morrison, and A. J. Smits, Further observations on the mean velocity distribution in fully developed pipe flow, *J. Fluid Mech.* **501**, 135 (1999).
- [6] P. A. Monkewitz, K. A. Chauhan, and H. M. Nagib, Self-consistent high-Reynolds-number asymptotics for zero-pressure-gradient turbulent boundary layers, *Phys. Fluids* **19**, 115101 (2007).
- [7] E. L. Andreas, K. J. Claffey, R. E. Jordan, C. W. Fairall, P. S. Guest, P. O. G. Persson, and A. A. Grachev, Evaluations of the von Kármán constant in the atmospheric surface layer, *J. Fluid Mech.* **559**, 117 (2006).
- [8] M. Lee and R. D. Moser, Direct numerical simulation of turbulent channel flow up to $Re_\tau \approx 5200$, *J. Fluid Mech.* **774**, 395 (2015).
- [9] Y. Yamamoto and Y. Tsuji, Numerical evidence of logarithmic regions in channel flow at $Re_\tau = 8000$, *Phys. Rev. Fluids* **3**, 012602(R) (2018).
- [10] A. Obukhov, Turbulence in thermally inhomogeneous atmosphere, *Trudy Inst. Teor. Geofiz. Akad. Nauk SSSR* **1**, 95 (1946).
- [11] A. Monin and A. Obukhov, Basic laws of turbulent mixing in the surface layer of the atmosphere, *Contrib. Geophys. Inst. Acad. Sci. USSR* **151**, e187 (1954).
- [12] R. B. Stull, *An Introduction to Boundary Layer Meteorology* (Springer Science & Business Media, Berlin, 1988), Vol. 13.
- [13] J. W. Deardorff, Parameterization of the planetary boundary layer for use in general circulation models, *Mon. Weather Rev.* **100**, 93 (1972).
- [14] I. Troen and L. Mahrt, A simple model of the atmospheric boundary layer; sensitivity to surface evaporation, *Boundary-Layer Meteorol* **37**, 129 (1986).
- [15] A. Holtslag and B. Boville, Local versus nonlocal boundary-layer diffusion in a global climate model, *J. Clim.* **6**, 1825 (1993).
- [16] J.-F. Louis, A parametric model of vertical eddy fluxes in the atmosphere, *Boundary-Layer Meteorol* **17**, 187 (1979).
- [17] L. Mahrt, Stratified atmospheric boundary layers and breakdown of models, *Theor. Comput. Fluid Dyn.* **11**, 263 (1998).
- [18] A. A. Grachev, E. L. Andreas, C. W. Fairall, P. S. Guest, and P. O. G. Persson, Similarity theory based on the Dougherty–Ozmidov length scale, *Q. J. R. Meteorol. Soc.* **141**, 1845 (2015).
- [19] P. Viterbo, A. Beljaars, J.-F. Mahfouf, and J. Teixeira, The representation of soil moisture freezing and its impact on the stable boundary layer, *Q. J. R. Meteorol. Soc.* **125**, 2401 (1999).
- [20] S. Basu, F. Porté-Agel, E. Fofoula-Georgiou, J.-F. Vinuesa, and M. Pahlow, Revisiting the local scaling hypothesis in stably stratified atmospheric boundary-layer turbulence: An integration of field and laboratory measurements with large-eddy simulations, *Boundary-Layer Meteorol.* **119**, 473 (2006).
- [21] J. Cuxart, A. A. Holtslag, R. J. Beare, E. Bazile, A. Beljaars, A. Cheng, L. Conangla, M. Ek, F. Freedman, R. Hamdi *et al.*, Single-column model intercomparison for a stably stratified atmospheric boundary layer, *Boundary-Layer Meteorol.* **118**, 273 (2006).
- [22] G. Svensson and A. A. Holtslag, Analysis of model results for the turning of the wind and related momentum fluxes in the stable boundary layer, *Boundary-Layer Meteorol.* **132**, 261 (2009).
- [23] M. Momen, Baroclinicity in stable atmospheric boundary layers: Characterizing turbulence structures and collapsing wind profiles via reduced models and large-eddy simulations, *Quart. J. Royal Meteorol. Soc.* **148**, 76 (2022).
- [24] A. Holtslag, G. Svensson, P. Baas, S. Basu, B. Beare, A. Beljaars, F. Bosveld, J. Cuxart, J. Lindvall, G. Steeneveld *et al.*, Stable atmospheric boundary layers and diurnal cycles: Challenges for weather and climate models, *Bull. Am. Meteorol. Soc.* **94**, 1691 (2013).
- [25] J. Teixeira, B. Stevens, C. Bretherton, R. Cederwall, J. D. Doyle, J.-C. Golaz, A. A. Holtslag, S. Klein, J. K. Lundquist, D. A. Randall *et al.*, Parameterization of the atmospheric boundary layer: A view from just above the inversion, *Bull. Am. Meteorol. Soc.* **89**, 453 (2008).

- [26] G. Svensson, A. Holtslag, V. Kumar, T. Mauritsen, G. Steeneveld, W. Angevine, E. Bazile, A. Beljaars, E. De Bruijn, A. Cheng *et al.*, Evaluation of the diurnal cycle in the atmospheric boundary layer over land as represented by a variety of single-column models: The second GABLS experiment, *Boundary-Layer Meteorol.* **140**, 177 (2011).
- [27] M. M. Holland and C. M. Bitz, Polar amplification of climate change in coupled models, *Climate Dyn.* **21**, 221 (2003).
- [28] L. Mahrt, Stably stratified atmospheric boundary layers, *Annu. Rev. Fluid Mech.* **46**, 23 (2014).
- [29] J. Forrer and M. Rotach, On the turbulence structure in the stable boundary layer over the greenland ice sheet, *Boundary-Layer Meteorol.* **85**, 111 (1997).
- [30] M. Pahlow, M. B. Parlange, and F. Porté-Agel, On Monin-Obukhov similarity in the stable atmospheric boundary layer, *Boundary-Layer Meteorol.* **99**, 225 (2001).
- [31] C. L. Klipp and L. Mahrt, Flux–gradient relationship, self-correlation and intermittency in the stable boundary layer, *Q. J. R. Meteorol. Soc.* **130**, 2087 (2004).
- [32] Y. Cheng, M. B. Parlange, and W. Brutsaert, Pathology of Monin-Obukhov similarity in the stable boundary layer, *J. Geophys. Res. Atmos.* **110** (2005).
- [33] A. A. Grachev, C. W. Fairall, P. O. G. Persson, E. L. Andreas, and P. S. Guest, Stable boundary-layer scaling regimes: the sheba data, *Boundary-Layer Meteorol.* **116**, 201 (2005).
- [34] C. Yagüe, S. Viana, G. Maqueda, and J. M. Redondo, Influence of stability on the flux-profile relationships for wind speed, ϕ m, and temperature, ϕ h, for the stable atmospheric boundary layer, *Nonlin. Processes Geophys.* **13**, 185 (2006).
- [35] J. Dougherty, The anisotropy of turbulence at the meteor level, *J. Atmos. Terr. Phys.* **21**, 210 (1961).
- [36] R. Ozmidov, On the turbulent exchange in a stably stratified ocean. *Izv. Acad. Sci. USSR, Atmos. Oceanic Phys.* **1**, 861 (1965).
- [37] A. Gargett, T. Osborn, and P. Nasmyth, Local isotropy and the decay of turbulence in a stratified fluid, *J. Fluid Mech.* **144**, 231 (1984).
- [38] M. L. Waite, Stratified turbulence at the buoyancy scale, *Phys. Fluids* **23**, 066602 (2011).
- [39] D. Li, S. T. Salesky, and T. Banerjee, Connections between the Ozmidov scale and mean velocity profile in stably stratified atmospheric surface layers, *J. Fluid Mech.* **797**, 29 (2016).
- [40] Y. Cheng, Q. Li, S. Argentini, C. Sayde, and P. Gentine, A model for turbulence spectra in the equilibrium range of the stable atmospheric boundary layer, *JGR Atmos.* **125**, e2019JD032191 (2020).
- [41] C. Tong and M. Ding, Multi-point Monin–Obukhov similarity in the convective atmospheric surface layer using matched asymptotic expansions, *J. Fluid Mech.* **864**, 640 (2019).
- [42] Y. Cheng, Q. Li, D. Li, and P. Gentine, Logarithmic profile of temperature in sheared and unstably stratified atmospheric boundary layers, *Phys. Rev. Fluids* **6**, 034606 (2021).
- [43] O. Flores and J. Riley, Analysis of turbulence collapse in the stably stratified surface layer using direct numerical simulation, *Boundary-Layer Meteorol.* **139**, 241 (2011).
- [44] C. Anson and J. P. Mellado, Global intermittency and collapsing turbulence in the stratified planetary boundary layer, *Boundary-Layer Meteorol.* **153**, 89 (2014).
- [45] G. Ahlers, E. Bodenschatz, D. Funfschilling, S. Grossmann, X. He, D. Lohse, R. J. A. M. Stevens, and R. Verzicco, Logarithmic temperature profiles in turbulent Rayleigh–Bénard convection, *Phys. Rev. Lett.* **109**, 114501 (2012).
- [46] M. Hölling and H. Herwig, Asymptotic analysis of the near-wall region of turbulent natural convection flows, *J. Fluid Mech.* **541**, 383 (2005).
- [47] M. I. Budyko, *Evaporation Under Natural Conditions* (Gidrometeorizdat, Leningrad, 1948).
- [48] J. W. Deardorff, Numerical investigation of neutral and unstable planetary boundary layers, *J. Atmos. Sci.* **29**, 91 (1972).
- [49] Q. Li, P. Gentine, J. P. Mellado, and K. A. McColl, Implications of nonlocal transport and conditionally averaged statistics on Monin–Obukhov similarity theory and Townsend’s attached eddy hypothesis, *J. Atmos. Sci.* **75**, 3403 (2018).
- [50] Y. Cheng, C. Sayde, Q. Li, J. Basara, J. Selker, E. Tanner, and P. Gentine, Failure of Taylor’s hypothesis in the atmospheric surface layer and its correction for eddy-covariance measurements, *Geophys. Res. Lett.* **44**, 4287 (2017).

- [51] P. P. Sullivan, J. C. Weil, E. G. Patton, H. J. Jonker, and D. V. Mironov, Turbulent winds and temperature fronts in large-eddy simulations of the stable atmospheric boundary layer, *J. Atmos. Sci.* **73**, 1815 (2016).
- [52] S. K. Shah and E. Bou-Zeid, Direct numerical simulations of turbulent Ekman layers with increasing static stability: modifications to the bulk structure and second-order statistics, *J. Fluid Mech.* **760**, 494 (2014).
- [53] S. I. Gohari and S. Sarkar, Direct numerical simulation of turbulence collapse and rebirth in stably stratified Ekman flow, *Boundary-Layer Meteorol.* **162**, 401 (2017).
- [54] C. C. v. Heerwaarden, B. J. Van Stratum, T. Heus, J. A. Gibbs, E. Fedorovich, and J. P. Mellado, Microhh 1.0: A computational fluid dynamics code for direct numerical simulation and large-eddy simulation of atmospheric boundary layer flows, *Geosci. Model Dev.* **10**, 3145 (2017).
- [55] G. N. Coleman, J. Ferziger, and P. Spalart, Direct simulation of the stably stratified turbulent Ekman layer, *J. Fluid Mech.* **244**, 677 (1992).
- [56] F. T. Nieuwstadt, P. J. Mason, C.-H. Moeng, and U. Schumann, Large-eddy simulation of the convective boundary layer: A comparison of four computer codes, in *Turbulent Shear Flows 8* (Springer, New York, 1993), pp. 343–367.
- [57] A. N. Kolmogorov, The local structure of turbulence in incompressible viscous fluid for very large Reynolds numbers, *Dokl. Akad. Nauk SSSR* **30**, 299 (1941).
- [58] F. C. Bosveld, P. Baas, A. C. Beljaars, A. A. Holtslag, J. V.-G. de Arellano, and B. J. Van De Wiel, Fifty years of atmospheric boundary-layer research at Cabauw serving weather, air quality and climate, *Boundary-Layer Meteorol.* **177**, 583 (2020).
- [59] S. A. Cohn and W. M. Angevine, Boundary layer height and entrainment zone thickness measured by lidars and wind-profiling radars, *J. Appl. Meteorol.* **39**, 1233 (2000).
- [60] L. Choma, T. Musil, H. Némethová, J. Jevčák, P. Petříček, S. Makó, M. Pilát, and F. Balla, Comparative analysis of selected ceilometers for practice and academic purposes, in *2019 Modern Safety Technologies in Transportation (MOSATT)* (IEEE, New York, 2019), pp. 35–38.
- [61] J. C. Wyngaard, *Turbulence in the Atmosphere* (Cambridge University Press, Cambridge, UK, 2010).
- [62] W. K. George, Is there a universal log law for turbulent wall-bounded flows? *Philos. Trans. R. Soc. A* **365**, 789 (2007).
- [63] J. W. Deardorff, The counter-gradient heat flux in the lower atmosphere and in the laboratory, *J. Atmos. Sci.* **23**, 503 (1966).
- [64] K. Yoon and Z. Warhaft, The evolution of grid-generated turbulence under conditions of stable thermal stratification, *J. Fluid Mech.* **215**, 601 (1990).
- [65] S. Komori and K. Nagata, Effects of molecular diffusivities on counter-gradient scalar and momentum transfer in strongly stable stratification, *J. Fluid Mech.* **326**, 205 (1996).
- [66] E. Blay-Carreras, E. Pardyjak, D. Pino, D. Alexander, F. Lohou, and M. Lothon, Countergradient heat flux observations during the evening transition period, *Atmos. Chem. Phys.* **14**, 9077 (2014).
- [67] I. Marusic, J. P. Monty, M. Hultmark, and A. J. Smits, On the logarithmic region in wall turbulence, *J. Fluid Mech.* **716**, R3 (2013).
- [68] J. A. Businger, J. C. Wyngaard, Y. Izumi, and E. F. Bradley, Flux-profile relationships in the atmospheric surface layer, *J. Atmos. Sci.* **28**, 181 (1971).
- [69] See Supplemental Material at <http://link.aps.org/supplemental/10.1103/PhysRevFluids.8.114602> for more atmospheric observations.
- [70] V. M. Gryanik, C. Lüpkes, A. Grachev, and D. Sidorenko, New modified and extended stability functions for the stable boundary layer based on SHEBA and parametrizations of bulk transfer coefficients for climate models, *J. Atmos. Sci.* **77**, 2687 (2020).
- [71] T. Foken, 50 years of the Monin–Obukhov similarity theory, *Boundary-Layer Meteorol.* **119**, 431 (2006).
- [72] H. A. Panofsky, Determination of stress from wind and temperature measurements, *Q. J. Royal Met. Soc.* **89**, 85 (1963).
- [73] G. Kramm, D. J. Amaya, T. Foken, and N. Mölders, Hans A. Panofsky’s integral similarity function—At fifty, *Atmos. Clim. Sci.* **3**, 581 (2013).
- [74] D. Krug, W. J. Baars, N. Hutchins, and I. Marusic, Vertical coherence of turbulence in the atmospheric surface layer: Connecting the hypotheses of Townsend and Davenport, *Boundary-Layer Meteorol.* **172**, 199 (2019).

- [75] F. T. Nieuwstadt, The turbulent structure of the stable, nocturnal boundary layer, *J. Atmos. Sci.* **41**, 2202 (1984).
- [76] L. Mahrt, The near-calm stable boundary layer, *Boundary-Layer Meteorol.* **140**, 343 (2011).
- [77] S. Pope, *Turbulent Flows* (Cambridge University Press, Cambridge, UK, 2000).
- [78] O. Williams, T. Hohman, T. Van Buren, E. Bou-Zeid, and A. J. Smits, The effect of stable thermal stratification on turbulent boundary layer statistics, *J. Fluid Mech.* **812**, 1039 (2017).
- [79] D. Caldwell, C. Van Atta, and K. Helland, A laboratory study of the turbulent Ekman layer, *Geophys. Fluid Dyn.* **3**, 125 (1972).
- [80] G. N. Coleman, J. Ferziger, and P. Spalart, A numerical study of the turbulent Ekman layer, *J. Fluid Mech.* **213**, 313 (1990).
- [81] <http://www.cesar-database.nl>.